Multiscale patterning of plasmonic metamaterials

JOEL HENZIE[1], MIN HYUNG LEE[1] AND TERI W. ODOM[1,2]*

[1]Department of Chemistry, Northwestern University, Evanston, Illinois 60208, USA
[2]Department of Materials Science and Engineering, Northwestern University, Evanston, Illinois 60208, USA
*e-mail: todom@northwestern.edu

Published online: 19 August 2007; doi:10.1038/nnano.2007.252

The interaction of light with surface plasmons—collective oscillations of free electrons—in metallic nanostructures has resulted in demonstrations of enhanced optical transmission[1], collimation of light through a subwavelength aperture[2], negative permeability and refraction at visible wavelengths[3,4], and second-harmonic generation from magnetic metamaterials[5]. The structures that display these plasmonic phenomena typically consist of ordered arrays of particles or holes with sizes of the order of 100 nm. However, surface plasmons can interact with each other over much longer distances, so the ability to organize nanoscale particles or holes over multiple length scales could lead to new plasmonic metamaterials with novel optical properties[6]. Here, we present a high-throughput nanofabrication technique—soft interference lithography—that combines the ability of interference lithography[7] to produce wafer-scale nanopatterns with the versatility of soft lithography[8], and use it to create such plasmonic metamaterials. Metal films perforated with quasi-infinite arrays of 100-nm holes were generated over areas greater than 10 cm^2, exhibiting sharp spectral features that changed in relative amplitude and shifted to longer wavelengths when exposed to increased refractive index environments. Moreover, gold nanohole arrays patterned into microscale patches exhibited strikingly different transmission properties; for instance, patches of nanoholes displayed narrow resonances (<14.5 nm full-width-at-half-maximum) that resulted in high refractive index sensitivities far exceeding those reported previously[9]. Soft interference lithography was also used to produce various infinite and finite-area arrays of nanoparticles, including patterns that contained optically distinct particles side by side and arrays that contained both metallic and dielectric materials.

Soft interference lithography (SIL) uses nanoscale patterns generated by interference lithography (IL) as high-quality masters for soft lithography. Figure 1a depicts a silicon master patterned with arrays of posts (diameter $d = 100$ nm, height $h = 400$ nm, pitch $a_0 = 400$ nm), which was then moulded against a transparent elastomer (polydimethylsiloxane, PDMS) to produce SIL PDMS photomasks. Hundreds of SIL PDMS masks can be replicated from a single IL-master without exhibiting observable defects. These masks were then placed in conformal contact with a thin layer of positive-tone photoresist on a Si(100) substrate and exposed to broadband ultraviolet light in a soft lithographic technique referred to as phase-shifting photolithography (Fig. 1b)[10,11]. At this point, the exposed photoresist was either developed to produce arrays of photoresist posts with the same lateral size, shape and pitch as the master (that is, infinite arrays), or subjected to a second exposure through a chromium mask in contact photolithography and developed to achieve microscale patterns of photoresist posts (that is, finite-sized arrays). Because the size of the patterned area of exposed photoresist posts has macroscale dimensions (~2 inch × 2 inch), we can align the vertical and top edges of this pattern with the Cr mask pattern (~1 inch × 1 inch) by hand. This simple method can achieve relatively good rotational alignment between nanoscale arrays and microscale patterns, with a misalignment of the arrays of less than 5°. We have also used a mask aligner to improve the misalignment to around 1°. Spatial alignment will be realized if the patterns on the Cr mask can be made commensurate with the photoresist post lattice. Subsequently, these photoresist patterns were transferred into free-standing metal or dielectric films perforated with holes using a soft nanofabrication procedure called PEEL (a combination of phase-shifting photolithography, etching, electron-beam deposition and lift-off of the film)[10,12,13]. Figure 1c shows that optically smooth, large-area (>10 cm^2) gold films perforated with 100-nm holes spaced by 400 nm can be produced by SIL.

To investigate how the properties of multiscale patterns of nanostructures depended on materials, we fabricated arrays of nanoholes in Au and Si. High-resolution scanning electron microscopy (SEM) images of Au and Si infinite nanohole arrays reveal that the topography of both patterned materials is similar (Fig. 2a,b); the 100-nm holes are circular, and the areas surrounding the holes are smooth. Figure 2c,d shows images of finite-sized arrays (or patches) of holes in Au and Si films that were generated by PEEL starting from 100-nm photoresist posts patterned into square arrays of circular regions ($d = 2.5$ μm, $a_0 = 4.5$ μm). In total, 1×10^7 hole-array patches were fabricated simultaneously, and each 2.5-μm patch contained around 30 nanoholes. Because the size and pitch of the circles on the Cr mask were incommensurate with the photoresist post lattice (400 nm), neighbouring patches had slightly different configurations of holes.

We characterized the optical properties of both infinite and finite-sized nanohole arrays by illuminating the films under normal incidence with collimated white light and collecting the transmitted light through a microscope objective coupled to a spectrometer. Bright-field optical images of Au and Si infinite nanohole arrays exhibited uniform intensities across the entire

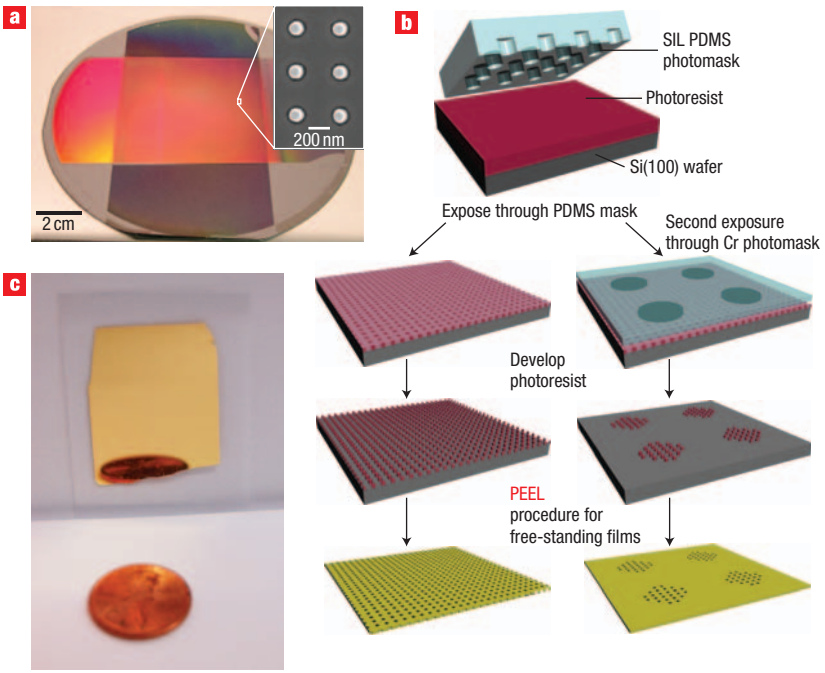

Figure 1 Soft interference lithography. a, Optical micrograph of a 14 cm^2 array of 100-nm-diameter Si posts (height and pitch = 400 nm) prepared by interference lithography; inset shows SEM image zoom. This pattern was used as a master for preparing SIL PDMS photomasks. **b**, Scheme depicting the fabrication procedure of infinite nanohole arrays and finite-sized arrays (patches) of holes. **c**, Optical micrograph of a large-area (dimensions: ~3 cm × 4 cm) gold film perforated with an array of 100-nm holes supported on glass. A reflection of the penny can be seen at the bottom of the gold film.

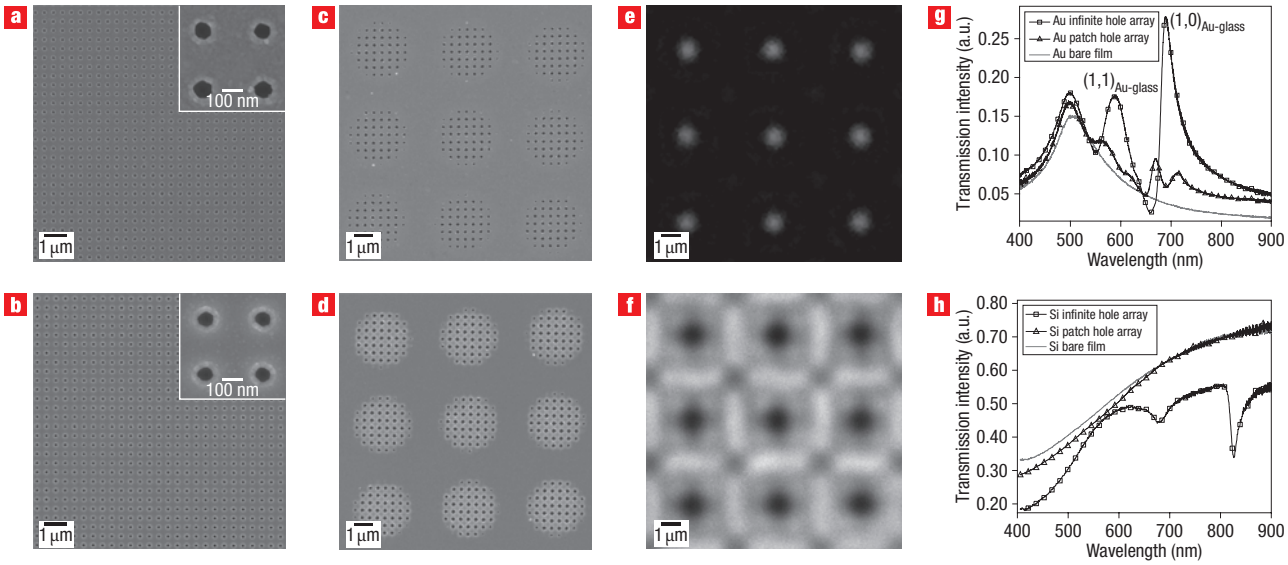

Figure 2 Optical properties of metal and dielectric films perforated with 100-nm holes. a–d, SEM images of infinite Au nanohole array (**a**), infinite Si nanohole array (**b**), Au patch nanohole array (**c**) and Si patch nanohole array (**d**). The nanohole patches were separated by $a_0 = 4.5$ μm. All films were 50 nm thick and supported on glass. **e**,**f**, Bright-field optical micrographs illuminated using a bandpass filter ($\lambda = 600$ nm $\pm$ 20 nm) of Au hole patches (**e**) and Si hole patches (**f**). **g**,**h**, Zero-order transmission spectra of infinite Au hole array (–□–), patch hole array (–Δ–) and solid film (——) (**g**); and infinite Si hole array (–□–), patch hole array (–Δ–) and solid film (——) (**h**).

field of view (see Supplementary Information, Fig. S1). In contrast, light from the finite-sized Au hole arrays was not uniform[14] and appeared to be localized to the central region of the patches (Fig. 2e). The transmitted light emerged with the narrowest lateral dimensions (768 nm) at wavelengths corresponding to surface plasmon polariton (SPP) resonances (see Supplementary Information, Fig. S2). These SPPs result from the resonant interaction between light and free electrons at a metal–dielectric

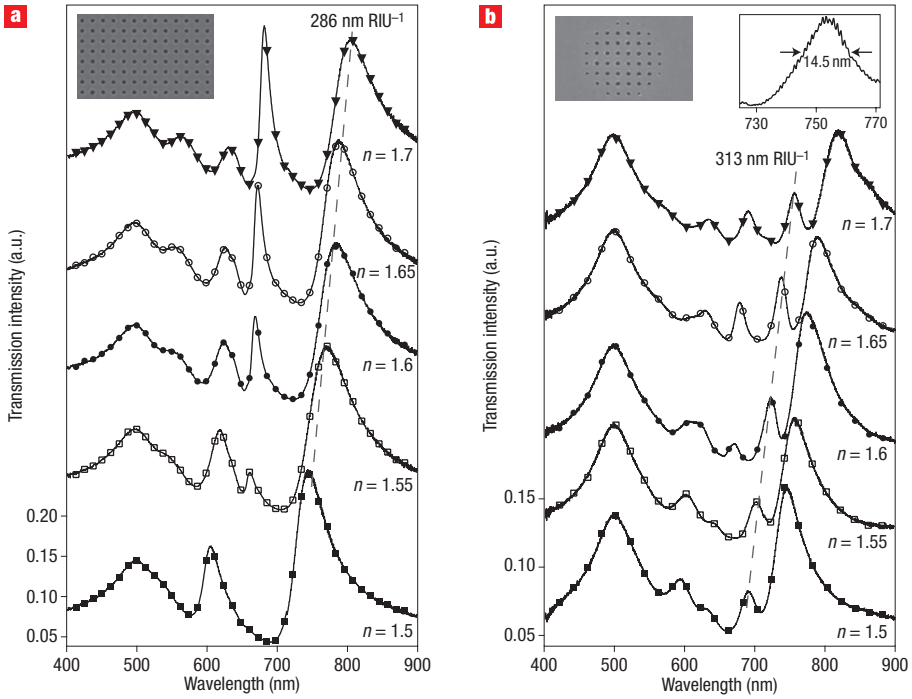

Figure 3 Refractive index sensing using Au nanohole arrays. **a**, Zero-order transmission of infinite Au hole arrays on glass in the presence of high-index immersion liquids ($n = 1.5000–1.7000$). The peaks shifted to longer wavelengths with higher n and split into multiple peaks at Wood's anomalies. The relative amplitude of peaks also changed as n increased. The inset image has dimensions 3.2 μm × 5.2 μm. **b**, Zero-order transmission of patches of Au nanoholes on glass in the presence of the same immersion liquids used in **a**. Both films were 50 nm thick. The right inset depicts the narrowest resonance from the 2.5-μm Au patches at $n = 1.7$. The left inset image has dimensions 3.2 μm × 5.2 μm.

interface. Although the geometries of the Au and Si patches were similar, their different material properties resulted in opposite effects, with light being concentrated in the former case and suppressed in the latter (Fig. 2f).

Figure 2g highlights the differences between the zero-order transmission spectra of infinite and finite-sized Au nanohole arrays. The intensity of the bulk plasmon resonance around $\lambda = 500$ nm was similar for all spectra. The infinite nanohole arrays exhibited peaks characteristic of SPP–Bloch waves (BW) at the Au–glass interface of $\lambda_{(1,0)} = 690$ nm and $\lambda_{(1,1)} = 588$ nm (ref. 15), where the subscripts (1,0) and (1,1) are integer pairs that define the particular order of the SPP–BW. The minimum in the spectra at $\lambda = 659$ nm can be associated with a Wood's anomaly (that is, light diffracted parallel to the surface of the film)[16]. Compared with the calculated transmission of hole arrays based only on geometry, SIL Au nanohole arrays exhibited enhanced optical transmission factors as large as 11, providing evidence that SIL can produce hole arrays of optical quality similar to those fabricated by focused ion-beam milling[1]. Strikingly, the spectra of Au patches of nanoholes exhibited a marked decrease in the relative intensity of the (1,0) SPP–BW resonance, which indicated that short-range coupling between holes was reduced, and the width of this peak was significantly narrower than that of the infinite array (full-width-at-half-maximum, FWHM = 18.3 versus 34.1 nm). Moreover, a new, narrow peak emerged at $\lambda = 660$ nm with a FWHM of 16.8 nm. In contrast, infinite Si nanohole arrays showed decreased transmission compared with solid films, and finite-sized arrays exhibited transmission slightly less than bare films (Fig. 2 h). Despite the different hole arrangements of individual patches, the spectra from single patches were identical because they contained, on average, the same number of holes.

Figure 3 displays how the narrow spectral features from SIL Au nanohole arrays can be exploited for highly sensitive refractive index (n) sensing. We controlled the dielectric environment on the top surface (previously air, $n = 1$) of films of infinite and finite-sized Au nanohole arrays by using immersion oils with different n. As expected for infinite Au nanohole arrays[17], the SPP–BW peaks shifted to longer wavelengths as n increased, but the bulk plasmon peak remained unchanged (Fig. 3a). Also, additional SPP resonances that were previously obscured by the bulk plasmon emerged, and existing peaks were redshifted and split by Wood's anomalies. On careful inspection, it is clear that as n increased, the relative amplitudes of peaks between 500 and 700 nm changed, which enables unexpected possibilities for using both the wavelengths of multiple resonances and their amplitudes to determine the refractive index of an analyte. A full theoretical analysis of the physical nature of the transmission resonances is beyond the scope of this paper. Recent numerical calculations have revealed, however, that at $n = 1.7$, the peak at $\lambda = 563$ nm is a localized resonance, the peak at $\lambda = 620$ nm is the (1,1) Au–oil resonance, the sharp peak at $\lambda = 681$ nm arises, in part, from first-order diffraction, and the peak around 800 nm can mostly be attributed to the (1,0) Au–oil resonance[18]. Finite-sized arrays of Au nanoholes under the same dielectric environments also exhibited trends similar to the infinite arrays (Fig. 3b), but noticeably, several peaks remained very narrow over the entire range of n tested; for example, the peak that shifted from $\lambda = 690$ nm ($n = 1.5$) to $\lambda = 756$ nm ($n = 1.7$) had an average FWHM of 14.8 ± 0.6 nm, which is the narrowest spectral width

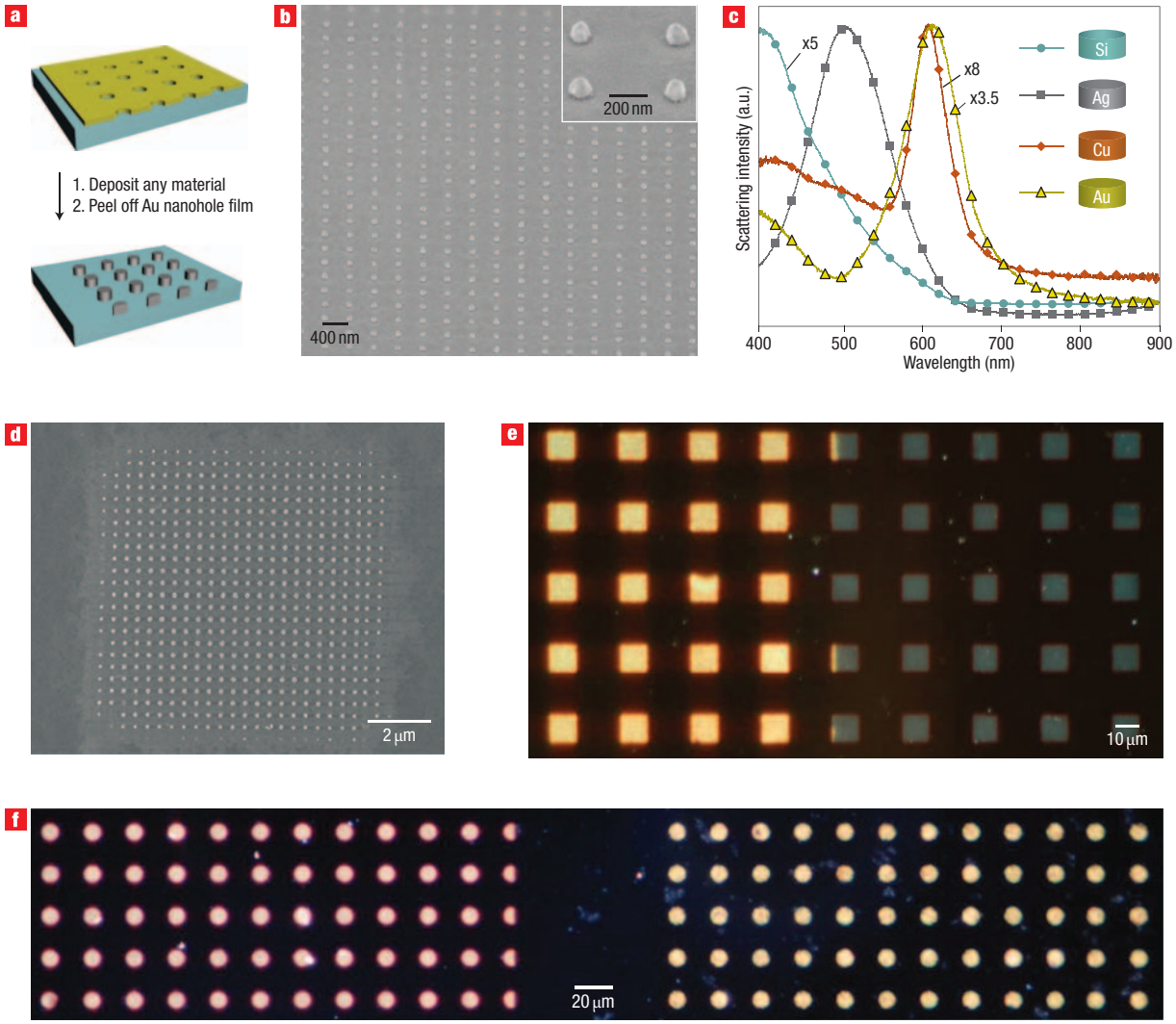

Figure 4 Infinite and multiscale nanoparticle arrays. a, Scheme depicting the fabrication of nanoparticle arrays using SIL Au nanohole films as deposition masks. The smallest pitch for all particle arrays was $a_0 = 400$ nm, and $d = 100$ nm. **b**, SEM image of an Au nanoparticle array ($h = 50$ nm) fabricated using an infinite nanohole film (inset shows image zoom). **c**, DF scattering spectra for metal (Ag, Cu, Au) and dielectric (Si) nanoparticles ($h = 50$ nm). The scattering peaks were scaled to the height of the Ag peak as indicated on the graph. **d**, SEM image of a 10 μm × 10 μm square of Au nanoparticles ($h = 65$ nm) fabricated using a nanohole patch film with a pitch of 25 μm. **e**, DF scattering image of Cu (left) and Ag (right) nanoparticles ($h = 15$ nm) fabricated on a different portion of the mask used in **d**. **f**, DF scattering image of Au (left) and Ag (right) nanoparticles ($h = 65$ nm) fabricated using a 10-μm circular nanohole patch film.

reported to date for a surface plasmon resonance excited using an incoherent light source.

One strategy to compare the sensitivity of different metallic nanostructure systems for refractive index sensing is to calculate their figure of merit (FOM), which is the shift per refractive index unit (RIU) divided by the width of the surface plasmon resonance (calculated in units of eV)[19]. The SPP–BW peaks for the infinite Au nanohole arrays were relatively broad (FWHM = 70 nm), and with a shift of 286 nm RIU^{-1}, the highest FOM achieved was ~ 4.1 for the $\lambda_{(1,0)}$ resonance (Fig. 3a). The resonances for the Au patches shifted slightly more than the infinite array (313 nm RIU^{-1}; or 0.747 eV RIU^{-1}), and considering the peak nearest to $\lambda_{(1,0)}$ (whose FWHM = 14.5 nm at $n = 1.7$; or 0.032 eV), a FOM as large as 23.3 was produced. This value far exceeds the range reported for metal nanoparticles (FOM = 0.9–5.4; ref. 9) as well as that of a recently reported structure made from a metal film deposited over polystyrene spheres[20]. Surprisingly, the best architecture for arrays of patches for refractive-index sensing consisted of patches that were close enough (for example, $a_0 = 4.5$ μm) to interact with each other. Patches of similar and larger sizes (2.5, 5 and 10 μm) separated edge to edge by 15 μm (that is, $a_0 = 17.5$–25 μm), a distance greater than the Au-plasmon decay length, did not support any new resonances. Significantly, as the number of holes increased, the patches began to exhibit features characteristic of the infinite array (see Supplementary Information, Figs S3 and S4).

To establish further the versatility of the nanofabrication approach, we used SIL to fabricate large-area arrays of metallic and dielectric nanoparticles. Figure 4a illustrates how SIL Au nanohole films can function as deposition masks to create arrays of nanoparticles. Figure 4b depicts a portion of an array of Au nanoparticles ($d = 100$ nm, $h = 50$ nm) supported on a glass

substrate (no adhesion layer is necessary) with the same pitch ($a_0 = 400$ nm) as the infinite nanohole mask. Nanoparticles of other single-component materials (Si, Ag, Cu) were fabricated and exhibited characteristic dark-field (DF) scattering peaks from ultraviolet to visible wavelengths (Fig. 4c). Calculations of their scattering properties were in good agreement with experiment, and indicated that nanoparticles on this pitch behaved as isolated particles (S. Zhou and G. C. Schatz, unpublished observations). Multilayered nanoparticles composed of alternating metal and dielectric layers were also fabricated by sequential deposition through nanohole masks (see Supplementary Information, Fig. S5). In addition, Au films perforated with nanohole patches were used as masks for multiscale patterning of different nanoparticles on the same substrate. Figure 4d is an SEM image of an Au nanoparticle array generated from a single 10-μm square hole patch within a patch array ($a_0 = 25$ μm). A different portion of this patch array-mask was also used to fabricate 100-μm^2 areas of thin ($h = 15$ nm) Cu and Ag nanoparticles side by side; DF images indicated that some patches at the interface contained both materials (Fig. 4e). Finally, Fig. 4f shows that thicker ($h = 65$ nm) Au and Ag particles can be patterned into arrays of 10-μm circular regions.

In summary, we have demonstrated how a new multiscale nanofabrication technique can manufacture plasmonic metamaterials with unexpected optical properties. The scientific opportunities opened by such structures range from ultra-small light sources to highly sensitive refractive-index sensors. Moreover, by offering an accessible approach to multiscale nano manufacturing over tens of square centimetres, SIL could also be used to produce metal–dielectric nanostructures that exhibit negative refractive indices at optical wavelengths or plasmonic nanostructures that can detect and identify analytes with exquisite sensitivity.

METHODS

PREPARATION OF THE SIL PDMS PHOTOMASKS

The silicon SIL master was passivated with a fluorosilane (tridecafluoro-1,1,2,2-tetrahydrooctyl-1-trichlorosilane, Gelest) for 24 h in a vacuum dessicator. SIL PDMS masks were composite masks, made from two layers of PDMS, where the bottom layer was a stiffer version of 184-PDMS (called *h*-PDMS)[11]. The *h*-PDMS was spin-cast onto the SIL master and cured briefly (120 s, 70 °C); a liquid prepolymer of 184-PDMS (~3 mm) was then poured on the *h*-PDMS and cured for an additional 1.5 h.

SOFT INTERFERENCE LITHOGRAPHY

A positive-tone photoresist (Shipley 1805, diluted 1:3 with 1-methoxy-2-propyl acetate) was spin-cast on Si(100) wafers (5,000 r.p.m., 40 s) and baked (90 s, 105 °C). The patterned side of the SIL PDMS mask was placed in conformal contact with the photoresist and exposed to broadband UV light (Quintel Q2000). The SIL PDMS mask was then removed, and the pattern was developed in a dilute solution of Microposit 351 (1:5 in water) to reveal a square array of photoresist posts with the same lateral spacing as the master. Microscale patterns (patches) of photoresist posts were fabricated by performing a second exposure using a chromium mask (solid areas were 2.5-μm-diameter circles on a 4.5-μm pitch) in contact photolithography before the developing step. The photoresist patches were then transferred into free-standing films of nanohole arrays using PEEL.

Cr (10 nm) was electron-beam deposited on the photoresist posts, and the resist was removed by sonicating the pattern in acetone to reveal round holes in the Cr film. Pyramidal pits were formed beneath the holes by etching the exposed Si with an anisotropic wet chemical etchant (23 g KOH, 33 mL isopropyl alcohol, in 100 mL H_2O at 72 °C). Then, 50 nm of gold or silicon was electron-beam deposited on this pattern to generate a film of nanohole arrays on the Si(100) surface, and pyramidal nanostructures in the pits[13]. The nanohole array was released from the Si substrate by wet chemical etching of the Cr underlayer (Transene), and was then transferred to a glass coverslip under water and dried for 24 h.

FABRICATION OF SINGLE AND MULTILAYERED NANOPARTICLES

Because the nanohole films produced by PEEL are inherently free-standing, they can easily be removed from any substrate by peeling them off in water. Hence, any materials combination can be deposited within the holes to form nearly cylindrical nanoparticles. Infinite arrays of metallic (Au, Ag, Cu) and dielectric (Si, Al_2O_3) materials were electron-beam evaporated on films ($h = 50$ nm) of nanohole arrays supported by a glass substrate. Finite arrays of nanoparticles were fabricated using films of circular ($d = 10$ μm) and square (side = 10 μm) patches; different materials could be patterned side by side using an additional large-area mask during deposition. Each component of the multilayered nanoparticles (Au/Al_2O_3, Al_2O_3/Au, $Au/Al_2O_3/Au$) was constructed simultaneously by depositing on the same large-area nanohole film but masking different areas to ensure the heights of the relevant layers in the nanoparticle were identical. The gold nanohole mask was removed by peeling it off in water or by placing a flat piece of PDMS in contact with the film for ~5 s and then gently removing it.

OPTICAL CHARACTERIZATION

Nanohole transmission spectra were collected using an inverted microscope (TE-2000U, Nikon). Collimated white light (divergence $<4°$) from a 100 W halogen source was passed through the nanohole film or solid film on glass, collected with a ×100 objective (NA = 0.5), and then focused onto an imaging spectrometer (Triax 522/LN_2-cooled CCD, Horiba Jobin Yvon). The data were corrected by dividing the film spectrum by the lamp transmission profile through the glass coverslip ($n = 1.523$). The index measurements were performed by placing a drop of immersion liquid ($n = 1.5000$, 1.5500, 1.6000, 1.6500 and 1.7000 ± 0.0005; Cargille Labs) between the gold nanohole films and the objective. The spectra for the patch arrays were collected from individual nanohole patches.

The scattering spectra of the nanoparticle arrays were collected using a standard transmission DF setup with the same microscope spectrometer used in the transmission experiments. The nanoparticle arrays on glass were illuminated through a DF condenser (NA = 0.8–0.95) and the scattered light was collected with a ×20 objective (NA = 0.75) and focused onto the spectrometer. The scattering data were corrected by dividing the lamp scattering profile of an etched glass coverslip. The refractive index measurements were performed by placing a drop of immersion liquid between the array and a ×100 objective (NA = 0.75).

Received 7 June 2007; accepted 16 July 2007; published 19 August 2007.

References

1. Ebbesen, T. W., Lezec, H. J., Ghaemi, H. F., Thio, T. & Wolff, P. A. Extraordinary optical transmission through sub-wavelength hole arrays. *Nature* **391,** 667–669 (1998).
2. Lezec, H. J. *et al.* Beaming light from a subwavelength aperture. *Science* **297,** 820–822 (2002).
3. Grigorenko, A. N. *et al.* Nanofabricated media with negative permeability at visible frequencies. *Nature* **438,** 335–338 (2005).
4. Dolling, G., Wegener, M., Soukoulis, C. M. & Linden, S. Negative-index metamaterial at 780 nm wavelength. *Opt. Lett.* **32,** 53–55 (2006).
5. Klein, M. W., Enkrich, C., Wegener, M. & Linden, S. Second-harmonic generation from magnetic metamaterials. *Science* **313,** 502–504 (2006).
6. Barnes, W. L., Dereux, A. & Ebbesen, T. W. Surface plasmon subwavelength optics. *Nature* **424,** 824–830 (2003).
7. Smith, H. I., Hector, S. D., Schattenburg, M. L. & Anderson, E. H. A new approach to high fidelity e-beam lithography based on an in-situ, global fiducial grid. *J. Vac. Sci. Technol. B* **9,** 2992–2995 (1991).
8. Xia, Y. & Whitesides, G. M. Soft lithography. *Angew. Chem. Int. Edn* **37,** 550–575 (1998).
9. Liao, H., Nehl, C. L. & Hafner, J. H. Biomedical applications of plasmon resonant metal nanoparticles. *Nanomedicine* **1,** 201–208 (2006).
10. Henzie, J., Barton, J. E., Stender, C. L. & Odom, T. W. Large-area nanoscale patterning: Chemistry meets fabrication. *Acc. Chem. Res.* **39,** 249–257 (2006).
11. Odom, T. W., Love, J. C., Wolfe, D. B., Paul, K. E. & Whitesides, G. M. Improved pattern transfer in soft lithography using composite stamps. *Langmuir* **18,** 5314–5320 (2002).
12. Gao, H., Henzie, J. & Odom, T. W. Direct evidence for surface plasmon-mediated enhanced light transmission through metallic nanohole arrays. *Nano Lett.* **6,** 2104–2108 (2006).
13. Henzie, J., Kwak, E. S. & Odom, T. W. Mesoscale metallic pyramids with nanoscale tips. *Nano Lett.* **5,** 1199–1202 (2005).
14. Bravo-Abad, J. *et al.* How light emerges from an illuminated array of subwavelength holes. *Nature Phys.* **2,** 120–123 (2006).
15. van der Molen, K. L., Segerink, F. B., van Hulst, N. F. & Kuipers, L. Influence of hole size on the extraordinary transmission through subwavelength hole arrays. *Appl. Phys. Lett.* **85,** 4316–4318 (2004).
16. Chang, S.-H., Gray, S. K. & Schatz, G. C. Surface plasmon generation and light transmission by isolated nanoholes and arrays of nanoholes in thin metal films. *Opt. Express* **13,** 3150–3165 (2005).
17. Krishnan, A. *et al.* Evanescently coupled resonance in surface plasmon enhanced transmission. *Opt. Commun.* **200,** 1–7 (2001).
18. McMahon, J., Henzie, J., Odom, T. W., Schatz, G. C. & Gray, S. K. submitted to Optics Express.

19. Sherry, L. J. *et al.* Localized surface plasmon resonance spectroscopy of single silver nanocubes. *Nano Lett.* **5,** 2034–2038 (2005).
20. Hicks, E. M. *et al.* Plasmonic properties of film over nanowell surfaces fabricated by nanosphere lithography. *J. Phys. Chem. B* **109,** 22351–22358 (2005).

Acknowledgements

This work was supported by the National Science Foundation (NSF) under NSF Award Number DMR-0632947 and the MRSEC program at the Materials Research Center under NSF Award Number DMR-0520513. This work made use of the NUANCE Center facilities, which are supported by NSF-MRSEC, NSF-NSEC and the Keck Foundation. We thank T. A. Savas and H. I. Smith for the Si masters made by interference lithography. We thank G. C. Schatz, S. K. Gray and J. McMahon for many discussions. T.W.O. is a DuPont Young Professor, an Alfred P. Sloan Research Fellow, a Cottrell Scholar of Research Corporation, and a David and Lucile Packard Fellow.

Correspondence and requests for materials should be addressed to T.W.O.
Supplementary information accompanies this paper on www.nature.com/naturenanotechnology.

Author contributions

J.H. and M.H.L. performed the experiments. J.H., M.H.L. and T.W.O. designed the experiments, analysed the results and co-wrote the manuscript.

Competing financial interests

The authors declare no competing financial interests.